Control Engineering Practice 35 (2015) 83–91

Contents lists available at ScienceDirect

Control Engineering Practice

journal homepage: www.elsevier.com/locate/conengprac

Multivariable maximum power point tracking for photovoltaic micro-converters using extremum seeking

Azad Ghaffari [a,*], Sridhar Seshagiri [b], Miroslav Krstić [c]

[a] Joint Doctoral Program (Aerospace and Mechanical) Between San Diego State University and University of California, San Diego, La Jolla, CA 92093-0411, USA
[b] Department of Electrical and Computer Engineering, San Diego State University, San Diego, CA 92182-1309, USA
[c] Department of Mechanical and Aerospace Engineering, University of California, San Diego, La Jolla, CA 92093-0411, USA

ARTICLE INFO

Article history:
Received 5 November 2013
Accepted 23 November 2014

Keywords:
Photovoltaic systems
Maximum power point tracking
Extremum seeking
DC–DC micro-converters

ABSTRACT

It is well-known that *distributed architectures* such as micro-converters and micro-inverters for photovoltaic (PV) systems can recover between 10% and 30% of annual performance loss or more that is caused by partial shading and/or module mismatch. In this work, we present a novel multivariable gradient-based extremum-seeking (ES) design to extract maximum power from an arbitrary micro-converter configuration of PV modules, that includes cascade and parallel connections. Conventional maximum power point tracking (MPPT) schemes for micro-converters (where each PV module is coupled to its own DC/DC converter) employ a distributed control, with one peak seeking scheme per each PV module, thereby requiring one control loop and two sensors per module (one each for current and voltage). By contrast, the scheme that we present employs a single control loop with just two sensors, one for the overall array output current and the other one for the DC bus voltage. This multivariable design provides more flexibility in tuning the parameters of the controller, and also takes into account interactions between PV modules. The computational effort of our design is not higher than that of the conventional scheme, and simulation and experimental results show that our proposed design outperforms the conventional one. Thus, our proposed design offers two benefits: (i) the balance-of-system (BOS) cost reduction as a result of the lower number of sensors, and (ii) improved performance, both contributing towards reduced average cost/watt, and enhancing the economic viability of solar.

1. Introduction

Maximum power point tracking (MPPT) is a technique for maximizing the energy extracted from PV modules. Over the years, many MPPT methods have been developed and implemented (Bratcu, Munteanu, Bacha, Picault, & Raison, 2011; Brunton, Rowley, Kulkarni, & Clarkson, 2010; Dhople, Ehlmann, Davoudi, & Chapman, 2010; Esram & Chapman, 2007; Hohm & Ropp, 2003; Jain & Agarwal, 2007; Kadri, Gaubert, & Champenois, 2011; Lei, Li, Chen, & Seem, 2010; Leyva et al., 2006; Miyatake, Veerachary, Toriumi, Fuji, & Ko, 2011; Moura & Chang, 2010; Pai, Chao, Ko, & Lee, 2011; Patel & Agarwal, 2009; Petrone, Spagnuolo, & Vitelli, 2011; Ramos-Paja, Spagnuolo, Petrone, Vitelli, & Bastidas, 2010). These methods vary in complexity, convergence speed, cost, range of effectiveness, implementation hardware, and popularity. Comprehensive comparative analyses of currently available techniques can be found in Esram and Chapman (2007), Hohm and Ropp (2003), and Jain and Agarwal (2007).

Extremum-seeking (ES) is a non-model-based real-time optimization algorithm (Ariyur & Krstić, 2003; Krstić & Wang, 2000; Wang & Krstić, 2000; Wang, Yeung, & Krstić, 1999) for systems with unknown dynamics that has been applied to a wide range of technical applications, including MPPT in PV systems (Bratcu et al., 2011; Brunton et al., 2010; Lei et al., 2010; Leyva et al., 2006; Moura & Chang, 2010). It offers the advantages of fast convergence and guaranteed stability over a range of environmental conditions, and yet is simple to implement, and hence very cost effective in terms of processing/hardware requirements.

With the exception of Bratcu et al. (2011), all existing work on ES applies the technique to PV systems whose cells receive the same irradiance level, i.e., have unimodal power characteristics. Recent works (for example, Dhople et al., 2010) concentrate on designing MPPT methods to track multiple peaks (non-unimodal power) under rapidly changing irradiance conditions, and the

* Corresponding author: Tel: +1 734 763 2227; fax: +1 734 647 3170.
E-mail addresses: aghaffari@ucsd.edu (A. Ghaffari), seshagir@engineering.sdsu.edu (S. Seshagiri), krstic@ucsd.edu (M. Krstić).

http://dx.doi.org/10.1016/j.conengprac.2014.11.007
0967-0661/

issues of partial shading and module mismatch. These studies have led to a growing interest in distributed architectures (also referred to as distributed power electronics), such as micro-converters (distributed DC/DC converters) and micro-inverters (distributed DC/AC converters) (Deline, Marion, Granata, & Gonzalez, 2011). While Bratcu et al. (2011) deals with ES design for micro-converters (one DC/DC converter for each module), it employs a scalar ES loop for each PV module. Two problems arise here. First, this scheme requires two sensors per module, current and voltage, which increases the levelized energy cost. Second, the coupling effect between PV modules is not addressed by this distributed control. Our current work shows that employing a multivariable MPPT algorithm instead of separate scalar ones solves these problems.

To the best of our knowledge, there are a limited number of multivariable MPPT schemes described in the literature, among which we refer the reader to Miyatake et al. (2011), Petrone et al. (2011), and Ramos-Paja et al. (2010). The last of these references (Ramos-Paja et al., 2010) uses a multivariable version of the popular Perturb and Observe (P&O) algorithm. Unlike scalar designs which require one current sensor for each module, the algorithm only requires a single current sensor on the DC bus. The operating point of the DC/DC converters are perturbed asynchronously, to minimize the possibility of converter interaction having a detrimental effect on the other modules. Closely related to Ramos-Paja et al. (2010) is the work in Petrone et al. (2011), where "extra variables" are employed in the classical P&O algorithm to overcome the limitation of scalar designs, which the authors say fail when the feasibility region is nonconvex. It is unclear how Petrone et al. (2011) compares with distributed architectures, with respect to power loss recovery in the case of module mismatch. Reference Miyatake et al. (2011) uses particle swarm optimization (PSO), which is an algorithm that employs multiple agents to "search" for the peak power. The paper does not describe the specific criteria used to select the number of agents and parameters of the PSO, or the conditions on the voltage and power boundary limits to stop the algorithm at Maximum Power Point (MPP). Also, in a PV system with a higher number of PV modules, the process of reinitialization and the tracking performance depend strongly on variable conditions like environmental factors, the nature of the PV modules, and the shading area. The authors claim that the required number of sensors are reduced to two, but to compute the pulse duration, the output voltage of each boost converter needs to be monitored by a separate sensor.

We present a multivariable gradient-based ES schemes with the following features:

- It is applied to micro-converter systems, and hence deals with the case of non-unimodal power characteristics, and deals specifically with the issue of module mismatch (for example, possibly different irradiance levels as a result of partially shaded conditions).
- The use of the non-model-based ES technique makes the design robust to partial knowledge of the system parameters and operating conditions.
- As opposed to scalar designs, our multivariable design only requires two sensors in all, for the overall PV system current, and the DC bus voltage. This is a significant reduction in hardware cost.
- Moreover, interactions between PV modules are inherently part of the multivariable design, and hence the transient performance is less-sensitive to environmental variable variations than a corresponding scalar design.
- The computational burden is of the same order as a scalar design, but with a slightly faster transient response than scalar ES designs, and significantly faster than non-ES based designs such as Miyatake et al. (2011).

In this expanded version of Ghaffari, Seshagiri, and Krstić (2012), we provide detailed guidelines for selection of the ES controller parameters, particularly the frequency distribution of the probing frequencies and bandpass frequencies of the lowpass filters. In addition, while the design was only validated by simulation in Ghaffari et al. (2012), here we present experimental results that demonstrate the effectiveness of the proposed algorithm against large step solar irradiance perturbations. Unlike several existing MPPT algorithms, ES requires no programming, and consists essentially of two filters, an oscillator, a multiplier, and an adder, all of which can be implemented using analog hardware (op-amps, resistors, capacitors). However, as is common in rapid prototyping, our implementation is done using the single-board dSPACE microcontroller.

The rest of this paper is organized as follows: the mathematical model of a PV module, along with a discussion of the DC/DC converter power electronics, is presented in Section 2. Section 3 introduces the scalar gradient-based ES scheme, presented for clarity for the case of a single module first, followed by how this is conventionally extended to the distributed micro-converter case. Our proposed multivariable gradient-based ES is presented and discussed in Section 4, along with some simulation and experimental results in Section 5, and a summary of our design and some concluding remarks in Section 6. A preliminary version of this paper was presented at the 2012 ACC (Ghaffari et al., 2012). The primary contribution of this work over Ghaffari et al. (2012) is the addition of experimental results to the simulation results that were presented therein.

2. Photovoltaic modules and power extraction

Our design and analysis are based on the standard PV module model described for example in Vachtsevanos and Kalaitzakis (1987), and shown schematically in Fig. 1. Each PV cell is modeled as an ideal current source of value I_{ph} in parallel with an ideal diode with voltage V_D. Electrical losses and contactor resistance are accounted for by the inclusion of the parallel and series resistances R_s and R_p respectively. The amount of generated current I_{ph} is dependent on the solar irradiance $\mathcal{S}$ and the temperature $\mathcal{T}$ through the following equation:

$$I_{ph} = \left(I_{ph}^r + k_i(\mathcal{T} - \mathcal{T}_r)\right)\left(\frac{\mathcal{S}}{1000}\right), \tag{1}$$

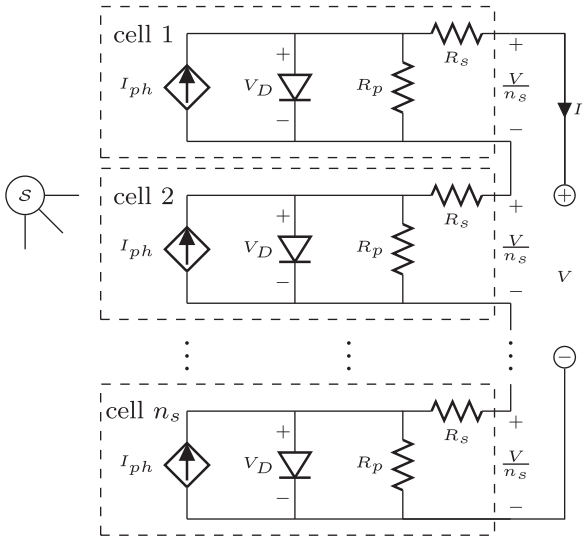

Fig. 1. Equivalent circuit of a PV module.

where I_{ph}^r is a reference short-circuit current, $\mathcal{T}_r$ a reference temperature, and k_i the short-circuit temperature coefficient. The diode models the effect of the semiconductor material and its $I-V$ characteristics are given by

$$I_D = I_0\left(\exp\left(\frac{V_D}{\mathcal{N}V_t}\right)-1\right), \tag{2}$$

$$I_0 = I_0^r\left(\frac{\mathcal{T}}{\mathcal{T}_r}\right)^3 \exp\left[\frac{E_g}{\mathcal{N}V_t}\left(\frac{1}{\mathcal{T}_r}-\frac{1}{\mathcal{T}}\right)\right], \quad V_t = \left(\frac{k\mathcal{T}}{q}\right) \tag{3}$$

where n_s, I_0^r, E_g and $\mathcal{N}$ are respectively the number of series PV cells in the module, the diode reference reverse saturation current, the semiconductor bandgap energy (barrier height), and the emission coefficient, the later three being cell material/construction dependent, V_t is the thermal cell voltage, and $k=1.38\times 10^{-23}$ J/K and $q=1.6\times 10^{-19}$ C are Boltzman's constant and the charge on an electron respectively. The cell model is described by the above equations along with KCL/KVL: $I=I_{ph}-I_D-V_D/R_p$, $V_D=V/n_s+R_sI$. One can then obtain PV module equation by considering n_s cells in series (each having cell thermal voltage V_t), so that the terminal $I-V$ relationship for the PV module is given by

$$I = I_{ph} - I_0\left[\exp\left(\frac{\frac{V}{n_s}+R_sI}{\mathcal{N}V_t}\right)-1\right] - \left[\frac{\left(\frac{V}{n_s}+R_sI\right)}{R_p}\right]. \tag{4}$$

For the sake of model development and performing simulations (done using the SimPowerSystems toolbox of Simulink), we pick the PV module 215N from Sanyo, with the following numerical values derived from the manufacturer's datasheet: $E_g=1.16$ eV, $\mathcal{N}=1.81$, $I_0^r=1.13\times 10^{-6}$ A, $I_{ph}^r=5.61$ A, $k_i=1.96$ mA/K, $\mathcal{T}_r=298.15$ K, $R_s=2.48$ mΩ, $R_p=8.7$ Ω, and the number of PV cells connected in series is $n_s=72$. The resulting $I-V$ and $P-V$ curves are shown in Fig. 2. As is clear from Fig. 2(b and d), the power-voltage ($P-V$) characteristic has a unique but $(\mathcal{T},\mathcal{S})$ dependent peak (V^*,P^*). It is the job of the MPPT algorithm to automatically track this peak. In many grid-tied PV systems (including our current work), this is done by means of a separate DC/DC power electronics stage that serves two functions: (i) regulating the output DC voltage at a (near) constant value, and (ii) extracting maximum power by forcing the PV module output V to equal V^*.

Fig. 3 shows this setup for a DC/DC converter stage, whose output voltage is maintained constant as $V_{\rm dc}$. The ratio between the input voltage V and the output voltage $V_{\rm dc}$ can be controlled by changing the duty cycle of the transistor switch, which serves as the control input d. We use a step-down or buck converter in our design. Under the assumption that the buck converter is working in Continuous Current Mode (CCM), and that the switching Pulse Width Modulation (PWM) frequency f_s is significantly higher than the bandwidth of the control loop, the buck converter input–output voltage and current relationships are given by the following (averaged) relations:

$$V = \frac{V_{\rm dc}}{\overline{\eta}d} \tag{5}$$

$$I = dI_{\rm dc}, \tag{6}$$

where $\overline{\eta}$ shows the power efficiency of the buck converter.

From (4), (5) and Fig. 2(b and d), it follows that at the MPP (V^*,P^*), the power $P=IV=f(V)V\stackrel{\rm def}{=}J(V)$, satisfies

$$g = \frac{\partial J}{\partial V}(V^*) = 0 \tag{7}$$

$$h = \frac{\partial^2 J}{\partial V^2}(V^*) < 0. \tag{8}$$

Also we have $\partial V/\partial d = -V_{\rm dc}/(\overline{\eta}d^2)$ then

$$\overline{g} = \frac{\partial J}{\partial d}(d^*) = -\frac{V_{\rm dc}}{\overline{\eta}(d^*)^2}g = 0 \tag{9}$$

$$\overline{h} = \frac{\partial^2 J}{\partial d^2}(d^*) = \frac{V_{\rm dc}^2}{\overline{\eta}^2(d^*)^4}h < 0. \tag{10}$$

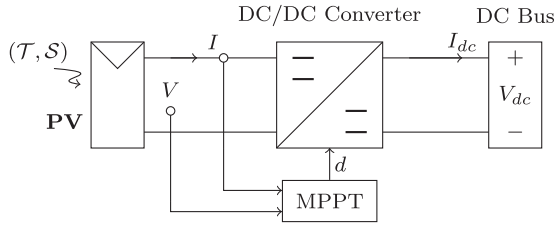

Fig. 3. PV module supplying power to a DC bus via a DC/DC converter.

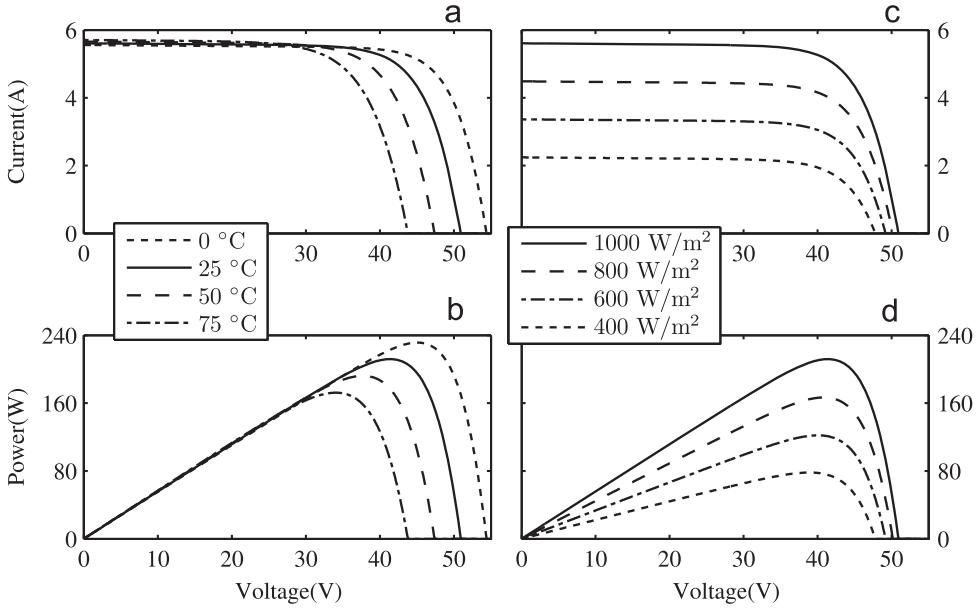

Fig. 2. Characteristic (a) $I-V$ and (b) $P-V$ for varying temperature, $\mathcal{S}=1000$ W/m^2. Characteristic (c) $I-V$ and (d) $P-V$ for varying irradiance, $\mathcal{T}=25$ °C.

Many MPPT techniques, including the classical perturb-and-observe (P&O) class of methods, and extremum-seeking (ES) techniques, are based on detecting the sign of the power gradient. The next section discusses scalar gradient-based ES in more detail.

3. Scalar gradient-based extremum seeking

Several authors have considered to use scalar gradient-based ES for the MPPT problem (Bratcu et al., 2011; Brunton et al., 2010; Lei et al., 2010; Leyva et al., 2006; Moura & Chang, 2010). Fig. 4 shows the basic setup of the scheme for the case of a single PV module, and its principal features have been explained fairly clearly in the aforementioned references, but we reproduce them here for the sake of completeness/clarity.

The injection of the small periodic perturbation $a\sin(\omega t)$ to the estimate $\hat{d}$ of the optimal pulse duration d^* results in a periodic power output P, whose DC component is removed by the wash-out filter $s/(s+\omega_h)$, with the resultant signal being in phase or out of phase with the perturbation according to whether $\hat{d}$ is less than or greater than d^* respectively. Multiplication of this signal by $2\sin(\omega t)/a$ and extracting the DC component of the product using the lowpass filter $\omega_l/(s+\omega_l)$ results in an estimate of the gradient of the cost function. Defining $\tilde{d}=\hat{d}-d^*$, and expanding P about its optimal value and using (7) and (8), we see that the ES design of

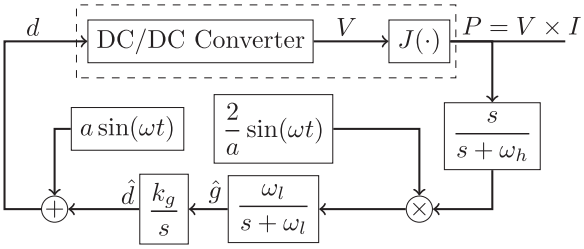

Fig. 4. Scalar extremum seeking for MPPT of a PV module.

Fig. 4 implements the gradient update law

$$\dot{\hat{d}} = k_g\hat{g} = k_g\frac{V_{dc}^2}{\overline{\eta}^2(d^*)^4}h\tilde{d}, \quad \hat{g} = \overline{h}\tilde{d}, \tag{11}$$

where h is the Hessian and it is the second derivative of the PV power map with respect to its terminal voltage. Design guidelines for selecting the parameters a, ω, ω_h, ω_l, and k_g can be found in Krstić and Wang (2000), but are mentioned here for sake of completeness. The frequency ω must be chosen small enough to ensure that the plant dynamics appear as a static nonlinearity from the viewpoint of the ES loop, and the filter frequencies chosen such that $\omega_h \le \omega_l \ll \omega$, so that the lowpass filter attenuates the perturbation frequency, whereas the highpass filter does not. The adaptation gain k_g and the amplitude a of the probing signal need to be "sufficiently small". Define

$$\omega = \epsilon\omega' \tag{12}$$

$$\omega_l = \epsilon\delta\omega_l' \tag{13}$$

$$\omega_h = \epsilon\delta\omega_h' \tag{14}$$

$$k_g = \epsilon\delta k_g', \tag{15}$$

where ϵ and δ are small positive real numbers, and $\omega', \omega_h', \omega_l'$ and k_g' are $O(1)$ positive real parameters. The analysis of Krstić and Wang (2000) shows that for sufficiently small ϵ, a, and δ, the output P converges to an $O(\epsilon+\delta+a)$-neighborhood of the MPP P^*.

The above design for a single module can be extended to the PV system shown in Fig. 5, that has m parallel strings, with each string having n modules in cascade (series). Since irradiance (and temperature to a lower extent) may vary between the modules, the peak power is not necessarily the same for all of them. This "module mismatch" therefore results in maximum powers for string architectures that are lower than the sum of the individual maximum powers of the modules, which in turn has led to the use of micro-converters, where each module is coupled with its own DC/DC converter. Micro-converter architectures can recover between 10% and 30% of annual performance loss caused due to module mismatch. The conventional

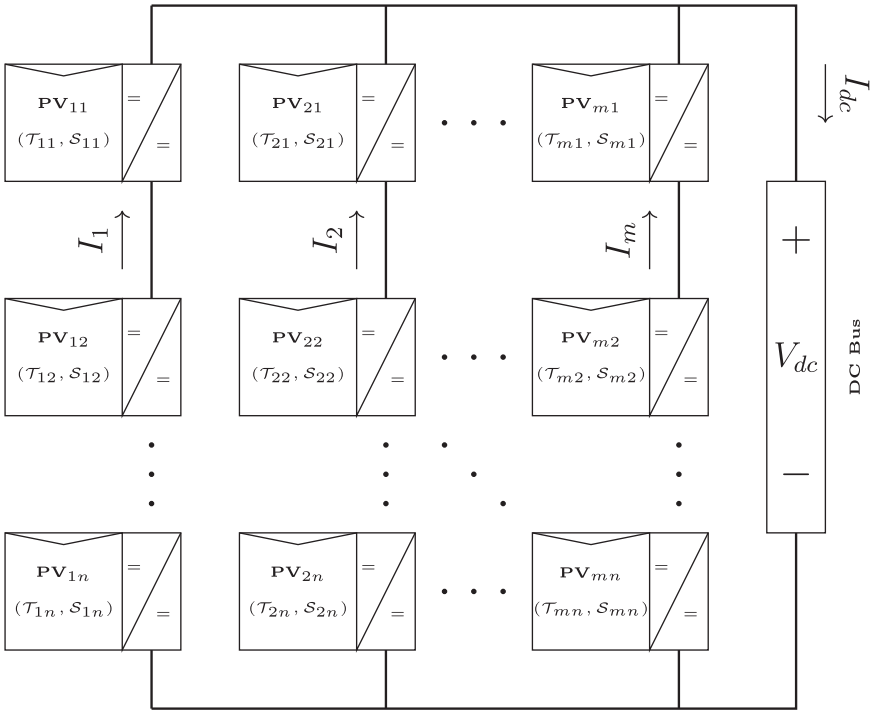

Fig. 5. PV system including m parallel strings. Each string has n PV modules in cascade.

way to implement the MPPT algorithm in micro-converters is to simply extend the preceding (scalar) MPPT design to each PV module, as shown in Fig. 6 for one string. In each string we therefore have n separate control loops, with no consideration to the interaction between the series modules. We also still have two sensors per module, that measure the module voltage and current. The multivariable control algorithm that we present in the next section alleviates both these issues; on one hand, it considers the interaction between modules, resulting in better performance, and in addition, uses just two sensors for the overall system, resulting in hardware reduction cost. The details of the actual design are presented in the next section.

4. Multivariable gradient-based extremum seeking

A cascade PV system is shown in Fig. 6. A DC/DC boost converter is assigned to each PV module to extract maximum power from the PV system. The output side of the converters are connected in series. The PV system is connected to the power grid through a DC/AC inverter which has its separate controller. It is assumed that the DC voltage at the input side of the inverter is held constant at V_{DC}. Assume that the voltage and the current ripple at the output side of converters are negligible. Applying electrical rules on the input side of the inverter gives

$$\sum_{j=1}^{n} V_{oj} = V_{DC} \tag{16}$$

$$I_{oj} = I_{DC}, \quad \forall j \in \{1,2,\ldots,n\}. \tag{17}$$

From (5), (6), and the $I-V$ functional dependence $I_j = f_j(V_j)$, the relation between the voltage $V = [V_1\ V_2 \cdots V_n]^T$ of PV modules and the pulse duration $D = [D_1\ D_2 \cdots D_n]^T$ is defined by n independent equations

$$\sum_{j=1}^{n} \overline{\eta} D_j V_j = V_{DC} \tag{18}$$

$$\frac{f_j(V_j)}{D_j} = I_{DC}, \quad \forall j \in \{1,2,\ldots,n\}. \tag{19}$$

One may obtain an explicit approximation of $f_i(V_i)$ as follows:

$$f_i(V_i) = I_{ph}^r \frac{\mathcal{S}_i}{1000} - I_0^r \exp\left(\frac{V_i}{n_s \mathcal{N} V_t^r}\right), \quad V_t^r = \left(\frac{k\mathcal{T}_r}{q}\right), \tag{20}$$

where $\mathcal{T} = \mathcal{T}_r$ and the effect of R_s and R_p is neglected. This means that for each set of pulse duration we have a unique set of voltages for PV modules. Moreover, we assume that each PV module has one bypass diode which means that the power map of a single PV module has one maximum point even under partial shading. This assumption along with (18) and (19) guarantees a single peak point for the overall power function defined as follows:

$$P = \sum_{i=1}^{n} P_i = V_{DC} I_{DC}. \tag{21}$$

The following observation is valid about the power.

Assumption 1. From (18) to (21), it follows that there exists $D^* \in \mathbb{R}^n$ such that

$$\frac{\partial P}{\partial D}(D^*) = 0 \tag{22}$$

$$\frac{\partial^2 P}{\partial D^2}(D^*) = H < 0, \quad H = H^T, \tag{23}$$

where H is the Hessian.

A block schematic of our proposed multivariable gradient-based ES is shown in Fig. 7. As is clear from the schematic, the design employs just one ES loop with two sensors for the overall system, one each for the DC bus voltage $V_{\rm dc}$ and the overall current $I_{\rm dc}$.

Fig. 8 shows the multivariable extension of the ES design that is described in Fig. 4, and its principal features are essentially the same as discussed in Section 3. The perturbation signals are defined as

$$S(t) = a[\sin(\omega_1 t) \quad \cdots \quad \sin(\omega_n t)]^T \tag{24}$$

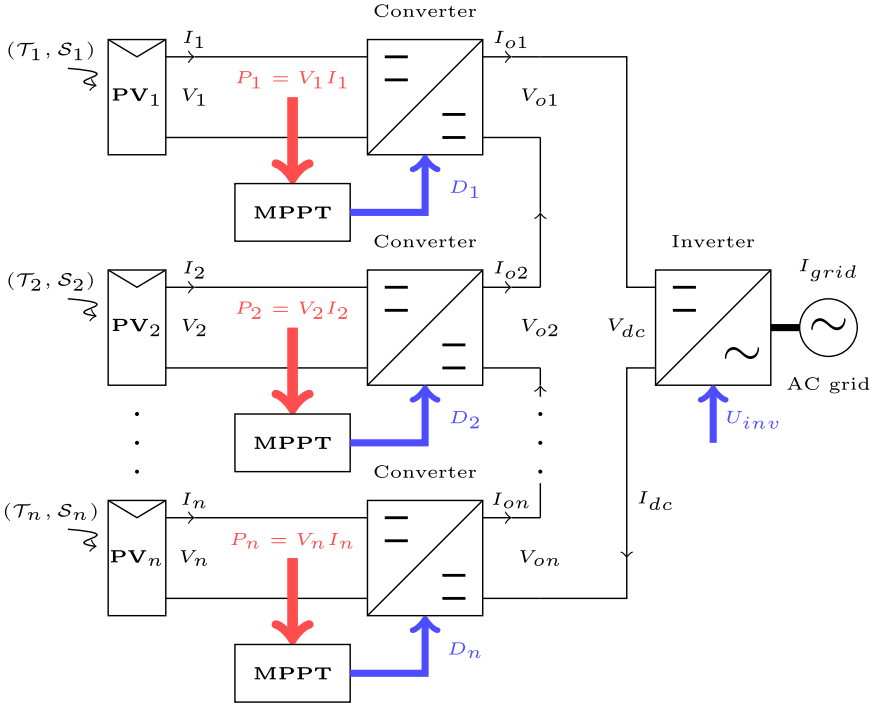

Fig. 6. Distributed MPPT for one string. One scalar ES loop is used for each PV module.

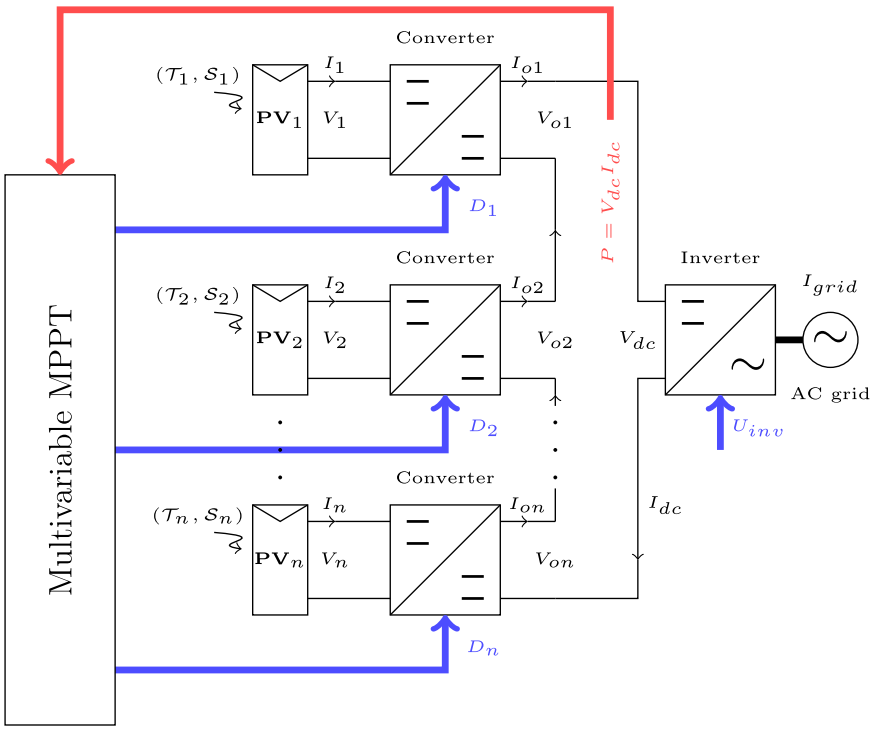

Fig. 7. Our proposed multivariable MPPT for PV system, just one multivariable ES loop is employed for all PV modules.

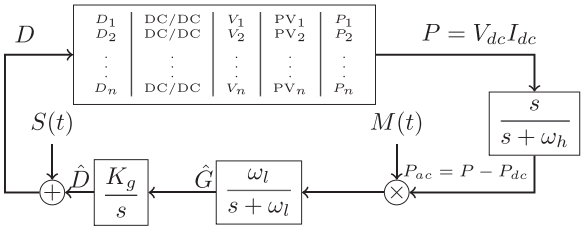

Fig. 8. Multivariable ES for MPPT of a PV system.

$$M(t)=\frac{2}{a}[\sin(\omega_1 t)\quad\cdots\quad\sin(\omega_n t)]^T, \tag{25}$$

where ω_i/ω_j are rational for all i and j, and a is a real number, with the frequencies chosen such that $\omega_i\neq\omega_j$ and $\omega_i+\omega_j\neq\omega_k$ for distinct i,j, and k. In particular, the design derives an estimate $\hat{G}$ of the gradient vector by adding a probing signal to the estimate

$$\hat{D}=[\hat{D}_1\ \hat{D}_2\ \cdots\ \hat{D}_n]^T$$

of the pulse duration vector (of all the DC/DC converters), and "filtering" the resultant power P through the process described before. With no additional information on the Hessian (and also for simplicity), we choose the amplitudes of the probing signals to all be the same value a. As before, smallness of the probing frequencies and the matrix gain K_g are ensured by selecting these as

$$\omega_i=\epsilon\omega_i',\quad i\in\{1,2,\ldots,n\} \tag{26}$$

$$K_g=\epsilon\delta K_g' \tag{27}$$

where ϵ and δ are small positive constants, ω_i' is a rational number, and elements of K_g' are $O(1)$ positive real parameters. The filter coefficients ω_l and ω_h are defined by (13) and (14). As before, it can be shown that for sufficiently small ϵ, δ, and a, and with $K_g>0$, the estimate $\hat{D}$ of the pulse duration vector and the output P converge to $O(\epsilon+\delta+a)$-neighborhoods of the optimal pulse duration $D^*=[D_1^*\ D_2^*\ \cdots\ D_n^*]^T$ and the MPP P^* respectively.

Applying Taylor series expansion to $P(D,t)$ at its maximum point, and noting that $\tilde{D}=\hat{D}-D^*$ and $D=D^*+\tilde{D}+S(t)$, we have

$$P=P^*+\frac{1}{2}\left(\tilde{D}+S(t)\right)^T H\left(\tilde{D}+S(t)\right)+R(\tilde{D}+S(t)). \tag{28}$$

where $\partial P(D^*)/\partial D=0$ and $R(\tilde{D}+S(t))$ stands for higher order terms in $\tilde{D}+S(t)$. We separate (28) into its averaged/DC part P_{dc} and oscillatory/AC part P_{ac} as follows:-

$$P=P_{dc}+P_{ac}, \tag{29}$$

where

$$P_{dc}=P^*+\frac{1}{2}\tilde{D}^T H\tilde{D}+R_{dc}(\tilde{D}) \tag{30}$$

$$P_{ac}=S^T(t)H\tilde{D}+\frac{1}{2}S^T(t)HS(t)+R_{ac}(\tilde{D}+S(t)), \tag{31}$$

where $R_{dc}(\tilde{D})$ and $R_{ac}(\tilde{D}+S(t))$ are higher order DC and AC terms, respectively. The high-pass filter attenuates the averaged/DC part of the power signal while keeps the high frequency part. Denoting

$$M(t)S^T(t)=I_{n\times n}+Z_{n\times n}, \tag{32}$$

where

$$Z_{jj}=-\cos(2\omega_j t) \tag{33}$$

$$Z_{jk}=\cos((\omega_j-\omega_k)t)-\cos((\omega_j+\omega_k)t),\quad j\neq k, \tag{34}$$

we obtain

$$M(t)P_{ac}=H\tilde{D}+ZH\tilde{D}+O(a), \tag{35}$$

where $O(a)$ contains terms of the order of a. From (28) we know that the gradient vector of the cost function is $G=\partial P/\partial\tilde{D}=H\tilde{D}$. Hence, the averaged/DC part of the multiplication of $M(t)$ and P_{ac} which equals to $H\tilde{D}$ is the estimate of the gradient vector of the cost function. An appropriate selection of the low-pass filter removes the oscillatory part of $M(t)P_{ac}$. Regardless of the vector length, n, the same low-pass filter on every channel of the gradient vector guarantees the averaging process and proper attenuation of

the high frequency terms. Referring to (33), (34), and (35) it is clear that the main harmonics in the estimate of the gradient vector are $2\omega_j$, $\omega_j \pm \omega_k$ for all distinct j and k. This observation motivates the following restriction on the choice of the low-pass filter frequency:

$$\omega_l \ll \{|\omega_j - \omega_k|\}, \qquad \forall j \neq k. \tag{36}$$

The differences between the scalar and multivariable designs become clear when one considers the update equations for the estimation error $\tilde{D} = \hat{D} - D^*$. In the multivariable case, we have

$$\dot{\tilde{D}} = K_g H \tilde{D}, \quad H := \frac{\partial^2 P}{\partial D^2}(D^*) \tag{37}$$

where H is the (negative definite) Hessian and $P = V_{dc} I_{dc}$. In the scalar ES design of Fig. 6 however, the above equation is replaced by

$$\dot{\tilde{D}} = k_g \mathcal{H} \tilde{D} \tag{38}$$

$$\mathcal{H} := \begin{bmatrix} \overline{h}_{PV_1} & 0 & 0 & \cdots & 0 \\ 0 & \overline{h}_{PV_2} & 0 & \cdots & 0 \\ \vdots & \vdots & \vdots & \ddots & \vdots \\ 0 & 0 & 0 & \cdots & \overline{h}_{PV_n} \end{bmatrix}, \tag{39}$$

where

$$\overline{h}_{PV_i} = \partial^2 P_i / \partial d_i^2, \quad P_i = V_i I_i \quad \forall i \tag{40}$$

(see Fig. 6), so that the equations are decoupled, and there is no way to affect the power extraction in one module by changing the pulse duration of the DC/DC converter of another module. In addition, the diagonal structure of $\mathcal{H}$ in the scalar case, coupled with the fact that this varies with irradiance, means that in the scalar design, the convergence rate of the parameters is very sensitive to partial shading, where the irradiance varies strongly from one module to another. The multivariable scheme, on the other hand, is less sensitive to the changes in the power–voltage characteristic of a specific module which results from variation of temperature or irradiance.

5. Simulation and experimental results

To show the effectiveness of the proposed multivariable MPPT algorithm in Fig. 7, we present both simulation and experimental results. Our simulation and experimental work were intentionally picked differently, and the latter choice was also influenced in part by the available hardware. For the simulation, we used a larger number of modules, and boost converters to prove the effectiveness of the proposed algorithm to handle non-minimum-phase systems with a larger number of PV modules. The experimental work was done with a more simple case of (fewer modules and) buck converters instead to simply experimentally validate the design features (such as the fact that no major redesign is required in the different cases) and showcase the performance improvement over scalar designs.

5.1. Simulation results

For the simulations, we consider a PV system with $m=2$ parallel strings and $n=3$ cascade modules in each string. The PV modules are model 215N from Sanyo, with datasheet parameters presented in Section 2. Guidelines for the selection of the ES parameters were presented in Ghaffari et al. (2012), and are reproduced here for completeness.

Selecting all the frequencies in a narrow range creates large overshoots and steady state errors in parameter estimation. However, choosing the frequencies in a wide range causes very different convergence rates in each channel. Since we set the lowpass filter frequency equal for all the channels, the amplitude of the perturbation signal with the lowest frequency reduces less than that with the highest frequency, which in turn results in a higher feedback gain for the low frequency channel, which derives the parameter faster to the optimal value. It is possible to tune the matrix gain elements with respect to the selected frequencies. What this means is that in order to have the same convergence rate for a wide range of selected frequencies, we can choose a higher gain for higher frequencies to compensate the effect of lowpass filter. We prefer to select the frequencies in a reasonable range, between 50% up and down of the central frequency. We remind the reader that the central frequency should be small enough in comparison to the PWM frequency. We suggest that this be of the order of less than 1% of the PWM frequency. The transient for the estimate of the gradient vector contains frequencies that include harmonics of $\omega_i - \omega_j$, for all distinct i and j. The bandwidth of the lowpass filter needs to be designed with respect to these values. We suggest selecting ω_l to be of the order of 5% of the least difference between the probing frequencies. The final step is selecting the cut-off frequency of the highpass filter, which we simply choose to be smaller than or equal to ω_l. Based on the preceding remarks, the numerical values of the design parameters are as presented in Table 1.

The temperature $\mathcal{T}$ is assumed to be equal to 25 °C for all modules throughout. The irradiance $\mathcal{S}$ is assumed to be equal to 1000 W/m^2 initially, with a step change to 500 W/m^2 for modules PV_{12} and PV_{23} at $t=0.5$ s and then back to 1000 W/m^2 at 1 s, so as to simulate partial shading on some modules. The output power of the entire system is shown in Fig. 9. It is clear from Fig. 9 that the multivariable algorithm performs a uniform and faster transient against step up or step down changes in the generated power.

At the beginning all PV modules and converters have the same settings, gains, and initial conditions. Also all modules are under the same irradiance and temperature. Hence, the transient of the

Table 1
Parameters used in the simulations.

Parameter	Value	Unit	Parameter	Value	Unit
f_s	100	kHz	V_{dc}	300	V
C_i	3	μF	C_o	220	μF
L	220	μH	d_0	0.5	–
K_g	0.01 $I_{6\times6}$	–	k_g	0.01	–
ω	7000	rad/s	a	0.01	–
ω_l	50	rad/s	ω_h	45	rad/s
ω_1	4500	rad/s	ω_4	5500	rad/s
ω_2	6500	rad/s	ω_5	7500	rad/s
ω_3	8500	rad/s	ω_6	9500	rad/s
m	2	–	n	3	–

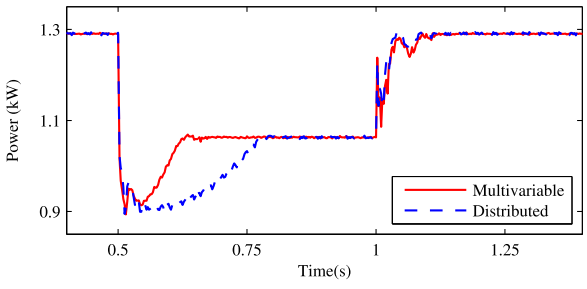

Fig. 9. Simulation results in a partial shading scenario. Extracted power by (solid red) multivariable and (dashed blue) distributed MPPT schemes. (For interpretation of the references to color in this figure caption, the reader is referred to the web version of this paper.)

scalar ES for all parameters is the same. On the other hand, multivariable ES shows different transients for each parameter which is happening because of different frequencies of the perturbation function in each channel. The lowest frequency shows the fastest response, along with a correspondingly larger overshoot. It is possible to tune matrix K_g such that all transients look the same.

When the modules in each string are partially shaded, the overall power level decreases. The multivariable ES design recovers from this power level change faster than the scalar version. As clear from Fig. 9, the power goes to the MPP in less than half the time needed for the scalar scheme.

The irradiance level of the partially shaded modules is returned to 1000 W/m^2 at $t=1$ s. At this point both schemes show a similar transient. It is concluded that the convergence rate of the multivariable scheme does not vary largely from step up to step down in power generation, which is not true for the scalar ES. It is clear that in the step down situation the scalar scheme shows a slower performance than the step up case.

5.2. Experimental results

Our hardware setup consists of two cascade PV modules connected to an active load which plays the role of the DC bus with $V_{dc}=5$ V, as shown in Fig 10. The PV modules are custom-made using 12 PV cells, with $P-V$ and $I-V$ characteristics shown in Fig. 11. We use dSPACE Control Desk Next Generation software and the DS1104 R&D Controller Board to implement our MPPT algorithms inside Simulink and interact with the DC/DC converters through Connector Panel CP1104. Also we use the "Power-Pole Boards" developed by the University of Minnesota for educational purposes, that are general purpose DC–DC converter boards, configured here as DC/DC buck converters, with external PWM signals generated by the DS1104. Each Power-pole board has a current sensor LA 25-NP to measure the inductor current which we use along with the capacitor ripple current measurement to calculate the DC bus current. We employ the DC bus current and DC bus voltage to measure the power supplied to the DC bus. The hardware setup is shown in Fig. 12. The numerical values of the parameters are as follows: $\omega=100\pi$ rad/s, $\omega_1=0.9\omega$, $\omega_2=\omega$, $\omega_l=\omega_h=\omega/20$, $k_g=2$, $K_g=k_g I_{2\times2}$, $a=0.05$, and $D_0=[0.7\ 0.7]^T$.

According to the theoretical results first-order lowpass filters are enough to separate the DC part of signals from their AC part. However, when we are implementing the algorithm on the experimental setup the first-order filters do not provide enough precision when separating DC and AC parts of the signals. Furthermore, to keep a constant group delay all over the bandpass of the filters we have chosen Bessel filters. According to our experiments, Bessel filters of order 5 or higher provide acceptable closed-loop performance. The PWM frequency is 100 kHz and the sampling time of the MPPT algorithm is 0.3 ms. The temperature of PV modules is 25° C and the modules are fully exposed to the sun from time 0 to 60 s and from 120 to 180 s. To simulate the effect of partial shading, PV_1 is covered with a plastic mat from time 60 to 120 s. When one module is partially shaded, the overall power level decreases. As clear from Fig. 13, the multivariable design recovers from this power level change faster than the distributed version. Furthermore, Fig. 14 shows that the adaptation process of the pulse duration in the multivariable method is faster

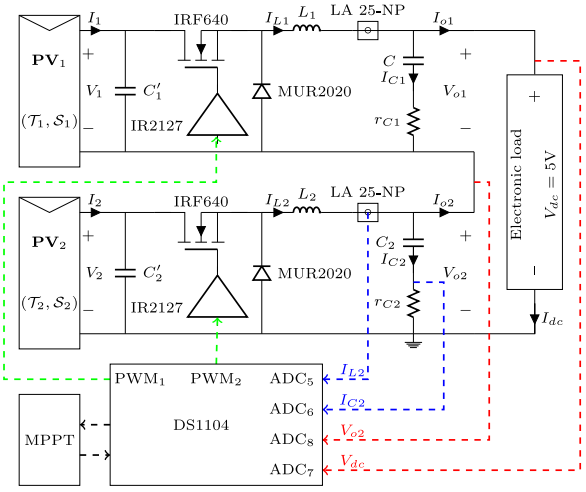

Fig. 10. Hardware configuration of the experimental setup.

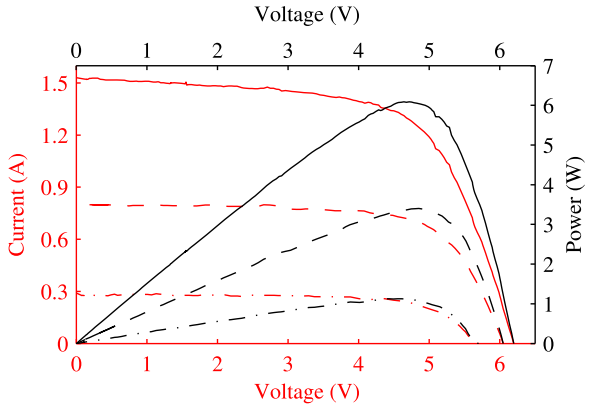

Fig. 11. Power and current maps of the custom-made PV modules used in the experiments for $\mathcal{T}=25$ °C. (Solid line) $\mathcal{S}=1000$ W/m^2, (dashed) $\mathcal{S}=520$ W/m^2, and (dash-dot) $\mathcal{S}=190$ W/m^2.

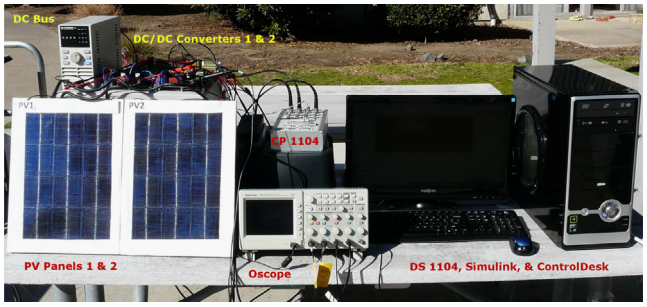

Fig. 12. Experimental setup.

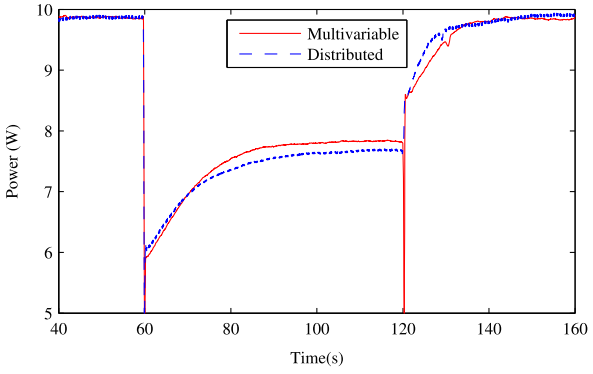

Fig. 13. Experimental results of the generated power in a partial shading scenario. (Solid red) Multivariable and (dashed blue) distributed MPPT algorithms. (For interpretation of the references to color in this figure caption, the reader is referred to the web version of this paper.)

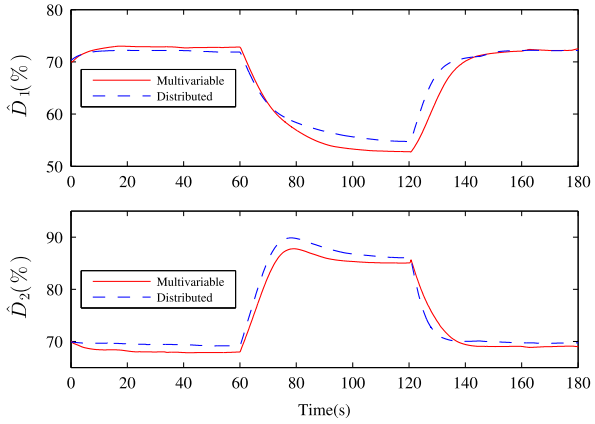

Fig. 14. Experimental results of the adaptation of the pulse duration. (Solid red) Multivariable and (dashed blue) distributed MPPT algorithms. (For interpretation of the references to color in this figure caption, the reader is referred to the web version of this paper.)

than the distributed design with the same MPPT gain in both algorithms.

The irradiance level of the partially shaded module is returned to normal level at $t=120$ s. At this point both schemes show a similar transient. It is concluded that the convergence rate of the multivariable scheme does not vary largely from step up to step down in power generation, which is not true for the distributed MPPT. It is clear that in the step down situation the distributed scheme shows a slower performance than the step up case. As expected, the experimental results are in keeping with the analytical and simulation results.

6. Conclusions

Using extremum seeking in a micro-converter configuration is a promising way to extract maximum power from a PV system. Conventionally used scalar gradient-based designs do so based on the generated power of each module. On one hand, this requires two sensors per module, and on the other hand, the dependence on the level and direction of changes of the individual powers causes different transients in the parameter updates, particularly in response to sudden irradiance changes caused by partial shading. The multivariable extremum seeking design that we present removes these drawbacks. Since the Hessian of the entire system (and not individual modules) defines the performance of the parameter update, this leads to more uniform transients in response to irradiance and temperature changes, lower power ripple than the scalar design, and improved overall performance. The scheme also only uses two sensors for the overall system, resulting in lower hardware cost. The dual advantages contribute towards reduced average cost/watt, enhancing the economic viability of solar. The effectiveness of the proposed design is validated by both analysis and experimental results.

References

Ariyur, K., & Krstić, M. (2003). *Real-time optimization by extremum seeking feedback*. New York: Wiley-Interscience.

Bratcu, A., Munteanu, I., Bacha, S., Picault, D., & Raison, B. (2011). Cascaded DC-DC converter photovoltaic systems: *Power optimization issues*. *IEEE Transactions on Industrial Electronics*, *58*, 403–411.

Brunton, S., Rowley, C., Kulkarni, S., & Clarkson, C. (2010). Maximum power point tracking for photovoltaic optimization using ripple-based extremum seeking control. *IEEE Transactions on Power Electronics*, *25*, 2531–2540.

Deline, C., Marion, B., Granata, J., & Gonzalez, S. (2011). *A performance and economic analysis of distributed power electronics in photovoltaic systems*. Technical Report, National Renewable Library.

Dhople, S., Ehlmann, J., Davoudi, A., & Chapman, P. (2010). Multiple-input boost converter to minimize power losses due to partial shading in photovoltaic modules. In *Proceedings of the IEEE Energy Conversion Congress and Exposition (ECCE)*.

Esram, T., & Chapman, P. (2007). Comparison of photovoltaic array maximum power point tracking techniques. *IEEE Transactions on Energy Conversion*, *22*, 439–449.

Ghaffari, A., Seshagiri, S., & Krstić, M. (2012). Power optimization for photovoltaic micro-converters using multivariable gradient-based extremum-seeking. In *Proceedings of the American Control Conference*.

Hohm, D. P., & Ropp, M. E. (2003). Comparative study of maximum power point tracking algorithms. *Progress in Photovoltaics: Research and Applications*, *11*, 47–62.

Jain, S., & Agarwal, V. (2007). Comparison of the performance of maximum power point tracking schemes applied to single-stage grid-connected photovoltaic systems. *IET Electric Power Applications*, *1*, 753–762.

Kadri, R., Gaubert, J.-P., & Champenois, G. (2011). An improved maximum power point tracking for photovoltaic grid-connected inverter based on voltage-oriented control. *IEEE Transactions on Industrial Electronics*, *58*, 66–75.

Krstić, M., & Wang, H.-H. (2000). Stability of extremum seeking feedback for general nonlinear dynamic systems. *Automatica*, *36*, 595–601.

Lei, P., Li, Y., Chen, Q., & Seem, J. (2010). Extremum seeking control based integration of MPPT and degradation detection for photovoltaic arrays. In *Proceedings of the American Control Conference*.

Leyva, R., Alonso, C., Queinnec, I., Cid-Pastor, A., Lagrange, D., & Martinez-Salamero, L. (2006). MPPT of photovoltaic systems using extremum seeking control. *IEEE Transactions on Aerospace and Electronic Systems*, *42*, 249–258.

Miyatake, M., Veerachary, M., Toriumi, F., Fuji, N., & Ko, H. (2011). Maximum power point tracking of multiple photovoltaic arrays: *A PSO approach*. *IEEE Transactions on Aerospace and Electronic Systems*, *47*, 367–380.

Moura, S., & Chang, Y. (2010). Asymptotic convergence through Lyapunov-based switching in extremum seeking with application to photovoltaic systems. In *Proceedings of the American Control Conference*.

Pai, F.-S., Chao, R.-M., Ko, S. H., & Lee, T.-S. (2011). Performance evaluation of parabolic prediction to maximum power point tracking for PV array. *IEEE Transactions on Sustainable Energy*, *2*, 60–68.

Patel, H., & Agarwal, V. (2009). MPPT scheme for a PV-fed single-phase single-stage grid-connected inverter operating in CCM with only one current sensor. *IEEE Transactions on Energy Conversion*, *24*, 256–263.

Petrone, G., Spagnuolo, G., & Vitelli, M. (2011). A multivariable perturb-and-observe maximum power point tracking technique applied to a single-stage photovoltaic inverter. *IEEE Transactions on Industrial Electronics*, *58*, 76–84.

Ramos-Paja, C. A., Spagnuolo, G., Petrone, G., Vitelli, M., & Bastidas, J. (2010). A multivariable MPPT algorithm for granular control of photovoltaic systems. In *Proceedings of the IEEE International Symposium on Industrial Electronics*.

Vachtsevanos, G., & Kalaitzakis, K. (1987). A hybrid photovoltaic simulator for utility interactive studies. *IEEE Transactions on Energy Conversion*, *EC-2*, 227–231.

Wang, H.-H., & Krstić, M. (2000). Extremum seeking for limit cycle minimization. *IEEE Transactions on Automatic Control*, *45*, 2432–2436.

Wang, H.-H., Yeung, S., & Krstić, M. (1999). Experimental application of extremum seeking on an axial-flow compressor. *IEEE Transactions on Control Systems Technology*, *8*, 300–309.